

Catalogue of Be/X-ray binary systems in the Small Magellanic Cloud: X-ray, optical & IR properties

M. J. Coe & J. Kirk

Physics and Astronomy, University of Southampton, SO17 1BJ, UK.

June 3 2015

ABSTRACT

This is a catalogue of ~ 70 X-ray emitting binary systems in the Small Magellanic Cloud (SMC) that contain a Be star as the mass donor in the system and a clear X-ray pulse signature from a neutron star. The systems are generally referred to as Be/X-ray binaries. It lists all their known binary characteristics (orbital period, eccentricity), the measured spin period of the compact object, plus the characteristics of the Be star (spectral type, size of the circumstellar disk, evidence for NRP behaviour). For the first time data from the Spitzer Observatory are combined with ground-based data to provide a view of these systems out into the far-IR.

Many of the observational parameters are presented as statistical distributions and compared to other similar populations (eg isolated Be & B stars) in the SMC, and to other Be/X-ray systems in the Milky Way. In addition previous important results are re-investigated using this excellently homogenous sample. In particular, the evidence for a bi-modality in the spin period distribution is shown to be even stronger than first proposed, and the correlation between orbital period and circumstellar disk size seen in galactic sources is shown to be clearly present in the SMC systems and quantised for the first time.

Key words: stars:neutron - X-rays:binaries

1 INTRODUCTION AND BACKGROUND

The Be/X-ray binary systems represent the largest subclass of all High Mass X-ray Binaries (HMXB). A survey of the literature reveals that of the ~ 240 HMXBs known in our Galaxy and the Magellanic Clouds (Liu, van Paradijs & van den Heuvel 2005), more than 50% fall within this class of binary. In fact, in recent years a substantial population of HMXBs has emerged in the Small Magellanic Cloud (SMC), comparable in number to the Galactic population, though unlike the Galactic population, all except one of the SMC HMXBs are Be star systems - referred to here as Be/X-ray systems. In these systems the orbit of the Be star and the compact object, presumably a neutron star, is generally wide and eccentric. X-ray outbursts are normally associated with the passage of the neutron star close to the circumstellar disk (Negueruela & Okazaki 2001), and generally are classified as Types I or II (Stella, White & Rosner 1986). The Type I outbursts occur periodically at the time of the periastron passage of the neutron star, whereas Type II outbursts are much more extensive and occur when the circumstellar

material expands to fill most, or all of the orbit. See Reig (2011) for a comprehensive review of these systems.

The population of such systems in the SMC is extremely valuable as it both provides a large sample (comparable to that known in the Milky Way), and one that is unimpaired by uncertainties in the distance and interstellar absorption. As such it provides an excellent laboratory to study the behaviour of both partners in these interacting binary systems. In this paper we will exclusively address the properties of these SMC sources, but we also note, in passing, that there is a smaller population in the Large Magellanic Cloud that is currently being identified through new X-ray surveys.

2 THE CATALOGUE

In this paper we present a summary of all such sources in the Small Magellanic Cloud. To be included in this catalogue the source must have exhibited clear evidence for X-ray pulsations at some stage. It is highly probable that there are many more systems that have yet to show such a feature, but already exist in X-ray surveys (see, for example, McBride et al, in prep.).

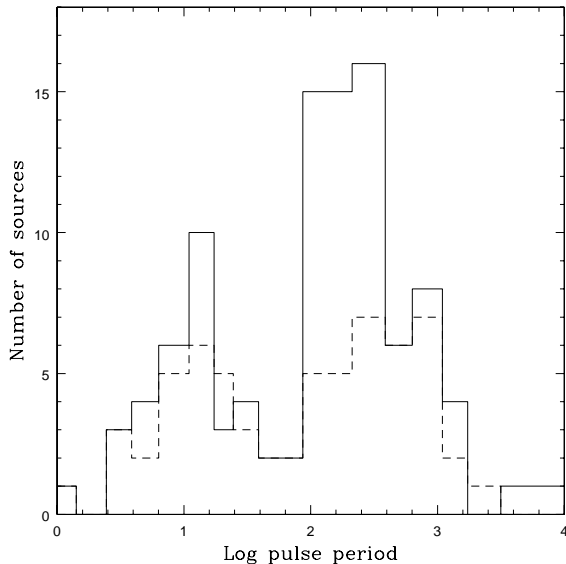


Figure 1. The distribution of pulse periods for all the Small Magellanic Cloud sources presented in this work (solid line). It is compared to the same distribution as presented in Knigge, Coe & Podsiadlowski (2011) (dashed line).

Presented in Table 2 and in Table 3 are the X-ray properties of the Be/X-ray systems in the SMC. Remarks pertaining to the contents of the tables are as follows:

- For convenience, all of the Magellanic Cloud sources are identified by a short name (column one in all the tables) first proposed by Coe et al. (2005). This identity is created simply from the acronym SXP (Small magellanic cloud X-ray Pulsar) followed by the pulse period in seconds to three significant figures. Where helpful, other official source names are listed in the tables. We have not attempted to provide a list of references associated with each source because an up to date literature review may be easily and accurately obtained through Simbad¹.

- Very few systems have reliable measurements of eccentricity - possibly the most secure measurement is one obtained from the Doppler shifting of the pulse period around an orbit. Those systems that have good values are the shorter orbital period systems and listed in Townsend et al. (2011) and the measurements are included here in Table 2, plus the more recent one for SXP 5.05 (Coe et al. 2015). None of the longer period sources in Table 3 have known eccentricities at this time.

- There is a column labelled "Other periods". These refer to periodic behaviour detected in the system that is believed not to be at the binary nor the pulse period. Examples of such characteristics are the presence of Non Radial Pulsations associated with the Be star (see, for example, Bird et al. (2012)), or a super-orbital period proposed to arise from a precessing accretion disk (Coe et al. 2013; Rajoelimanana, Charles & Udalski 2011).

Table 4 presents the optical and IR characteristics of the

mass donor star in the SMC systems. Because this star plays a major role in the observed X-ray characteristics of Be/X-ray systems it is important to include the known data on these components as well. This table contains the following columns:

- the proposed spectral identification of the Be star (obtained from a wide range of sources, all in published papers, all available through Simbad)
- the B&V magnitudes, widely available from several SMC surveys eg Zaritsky et al. (2002)
- the JHK magnitudes from the SMC survey carried out from the Japanese/South African Infra Red Survey Facility (IRSF) and published by Kato et al. (2007)
- the longer wavelength IR photometric values produced from the Spitzer SAGE surveys of the SMC (Bolatto et al. 2007; Gordon et al. 2011; Riebel et al. 2015)
- the measurements of the Equivalent Width (EW) of the H α emission line obtained from several observing runs at both the SALT and SAO 1.9m telescopes and summarised in Klus et al. (2014).

3 DISCUSSION TOPICS ARISING FROM THE CATALOGUE

3.1 The pulse period bimodality question

Figure 1 reveals that the increasing number of Be/X-ray systems in the Magellanic Clouds is strengthening the case presented by Knigge, Coe & Podsiadlowski (2011) that there is a clear bimodality in the pulse period distribution of these systems. Applying the same KMM test discussed in that paper to the updated SMC distribution results in a probability of 1.5×10^{-4} against this being a single distribution. This is compared to 6×10^{-4} for the smaller sample presented in Knigge, Coe & Podsiadlowski (2011).

The short and long spin sub-populations contribute about 40% and 60% to the total number, respectively, in this updated SMC sample. This is consistent with the ratio determined for the total Magellanic Clouds + Milky Way populations of 35% to 65% by Knigge, Coe & Podsiadlowski (2011).

Possible explanations for this bimodality currently includes two competing channels for producing supernovae and hence neutron stars (Heger et al. 2003), or maybe two modes of accretion (Cheng, Shao & Li 2014). The former suggestion leads to the possibility of confirmation by predicting different orbital eccentricities for the two populations, but currently the small number of confirmed values makes it difficult to say much at this time. This is one area where better observational results, perhaps through optical RV studies, could play a crucial role in understanding this bimodal-ity phenomenon.

3.2 IR properties of the SMC sources

The IR emission in Be/X-ray binary systems shows an excess over the standard stellar spectrum, and is believed to originate from free-free and bound-free emission in the circumstellar disk. It is the material in this disk that is responsible for fuelling the accretion on to the neutron star and hence generating the X-ray behaviour. It is also believed that the presence of the neutron star in orbit around the Be star can

¹ <http://simbad.u-strasbg.fr/simbad/>

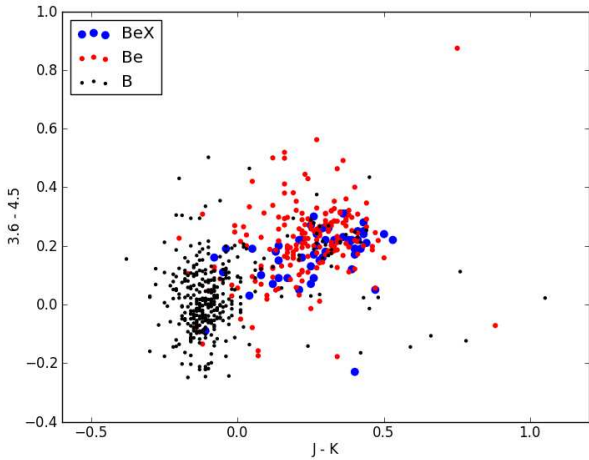


Figure 2. Colour-colour comparison plot of Be/X-ray sources, Be stars and B stars populations

constrain the growth and size of the circumstellar disk. One test of this hypothesis is to compare the IR emission from the Be stars in these systems with isolated Be stars, and also also isolated B and B[e] stars.

The isolated Be stars from the 2dFS catalogue (Evans et al. 2004) were plotted on the same colour-colour diagram (CCD) as the Be/X-ray sources (Figure 2). Both populations had data taken from the Sirius (Kato et al. 2007) and the SAGE-SMC catalogues (Gordon et al. 2011). In addition, the B type stars, again from the same 2dFS catalogue, were then added to this plot. This plot showed there to be great similarities in the distributions of the two populations of Be stars, but the disk-free B stars clearly fall elsewhere on this diagram. The B stars can be seen to occupy a region to the left of the CCD and it appears as though the Be and Be/X-ray sources branch off to the right of the main body of B stars. There are some outlying B stars which are distributed amongst the Be and Be/X-ray sources but these may have been incorrectly identified within the respective 2" search radii, or simply been previously misidentified as lacking a circumstellar disk. Since the disks in these systems can sometimes disappear, then Be stars can be thought to be B stars if observed at those times.

These 3 populations were then separated into their own CCDs so that the 3 distributions could be analysed more easily (Figure 3). This showed that although the Be stars had more spread in their (J-K) colours than the Be/X-ray stars, the Be/X-ray stars did, indeed, occupy a region within the main body of the Be type stars. The separation of the B type stars were however clear on the left of the plot but with a possible branch towards the Be and Be/X-ray region.

Due to the similarity between the distributions of the Be and Be/X-ray populations, 2-dimensional Kolmogorov-Smirnov (KS) tests were performed on the populations to determine the probability that they were drawn from the same parent population. The KS test used was the version written by Peter Yoachim² under Interactive Data Language (IDL). The comparison was made between these two distributions

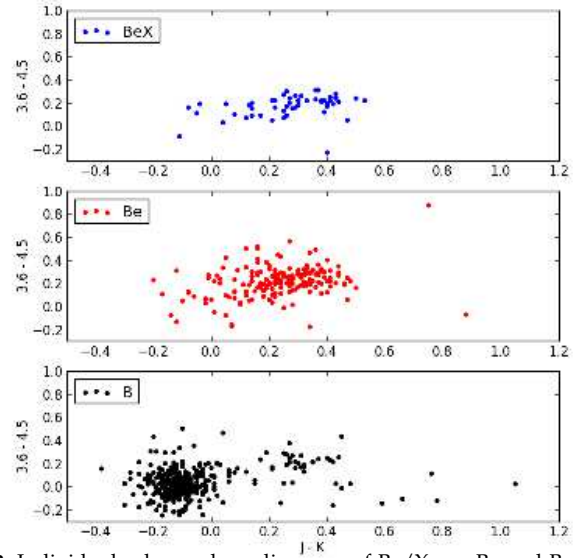


Figure 3. Individual colour-colour diagrams of Be/X-ray, Be and B populations

drawn from the (J-K) vs. (3.6–4.5 μ m) CCD. This returned a probability of 0.0174 that these two distributions were drawn from the same parent population, therefore not reaching the 3σ level. A similar test was performed on the Be/X-ray and B populations which returned a probability of 7.4×10^{-6} that they were drawn from the same parent population. So, though there is some suggestion of differences between the Be stars in Be/X-ray binaries and those in isolated systems, it is clear that both those groups are clearly distinguished from the isolated B stars. This is, of course, to be expected if the presence, or otherwise, of a circumstellar disk is the key ingredient in producing the IR excess. In fact, looking again at Figure 3, there is a strong suggestion that a significant part of the population of previously-identified B stars are incorrectly labelled as such, and that the Be star fraction should be higher.

Compact accreting objects are present in at least 2 Galactic sgB[e] systems (CI Cam (Bartlett et al. 2013) and IGR13618-4848 (Chaty & Rahoui 2012)) and X-ray detections have also been made of 2 sgB[e] stars in the MCs (Bartlett et al., in prep). Although it is not clear what is the origin of the X-ray emission in these systems (accretion or colliding winds), it was decided to extend this comparison to include known B[e] stars in the SMC. According to Bonanos et al. (2010) there are 7 such stars identified in the Spitzer/SAGE data. Because these stars are characterised by extended IR emission from a cool shell or toroid, the IR colour range was extended to (3.6–8.0 μ m). This reduced the size of the sample of B, Be & Be/X-ray binaries, but left enough to enable a meaningful comparison - see Figure 4.

The B[e] stars can be seen to occupy the upper right region of this plot. They are quite distinct from the other populations, and hence this CCD confirms that none of the Be/X-ray population included in this work includes a possible B[e] star. Clearly these kind of CCD plots provide good discriminators between the differing B star populations.

² <http://www.astro.washington.edu/users/yoachim>

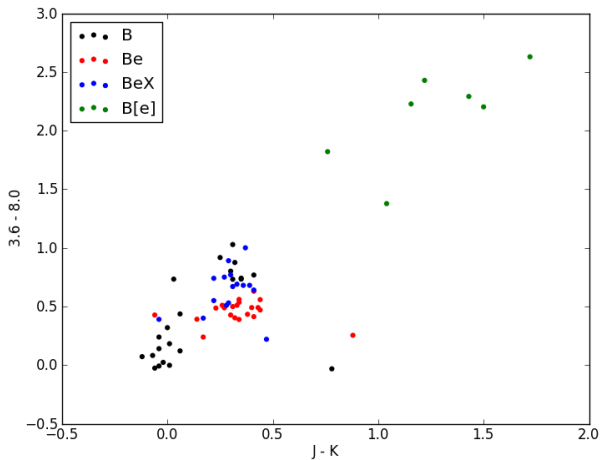


Figure 4. Colour-colour diagram of Be/X-ray, Be, B[e] and B populations.

3.3 Outbursts from SXP sources

The SMC was observed twice using Spitzer’s IRAC and MIPS instruments as part of the SAGE programme (Gordon et al. 2011) during two epochs in June and September 2008 (*epochs 1 & 2*, respectively). The IRAC catalogue contains observations of objects within the SMC in all 4 of its bands. In addition, this catalogue includes a third epoch, referred to as *epoch 0*, which used data taken from a previous study of the SMC performed in May 2005. This enabled the variability of the SXP objects to be studied on the two different timescales, a few months and a ~ 3 years.

Histograms of the change in magnitudes between epochs, for the IRAC bands, were plotted to check for any object showing significant variability (Figure 6). The long time scale between epoch 0 and the other two epochs (3 years) revealed that several objects’ magnitudes had substantially changed. The most significant case was that of SXP 18.3 (Table 1). The extreme X-ray variability of this object during this period of time has been reported by Schurch et al. (2009).

SXP 18.3 showed a change of one magnitude in the $4.5 \mu\text{m}$ band between epochs 1 and 2, with this large change occurring on a time scale of just 3 months. On a longer timescale changes of over a magnitude are present in both the $3.6 \mu\text{m}$ and $4.5 \mu\text{m}$ bands. The Optical Gravitational Lensing Experiment project has an SMC X-Ray variables monitoring system (OGLE-XROM) (Udalski 2008), and it obtained frequent I-band ($0.8 \mu\text{m}$) data. These data showed that SXP 18.3 is a very variable object which revealed strong flares in the I-band close to the time of the SAGE observations - see Figure 5.

In order to achieve near-simultaneity between the Spitzer data and the XROM data, the exact dates of the Spitzer individual observation were determined and the closest corresponding I band data for these dates were then found on XROM. OGLE/XROM data only exist for the first three Spitzer observations. This enabled the I band to be included in CCD plots of SXP 18.3 for these first 3 epochs. The resulting CCD showed great variation in this objects colour - see Figure 7

The flux values for the 3.6 and $4.5 \mu\text{m}$ bands used were

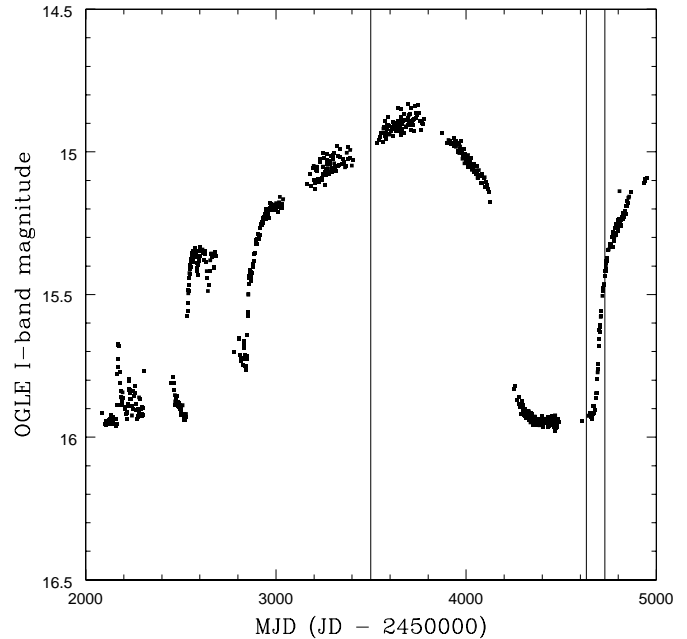


Figure 5. The OGLE I-band lightcurve of SXP 18.3. The epoch of the three first Spitzer/IRAC measurements are indicated by vertical lines. Later Spitzer observations are not covered by OGLE observations.

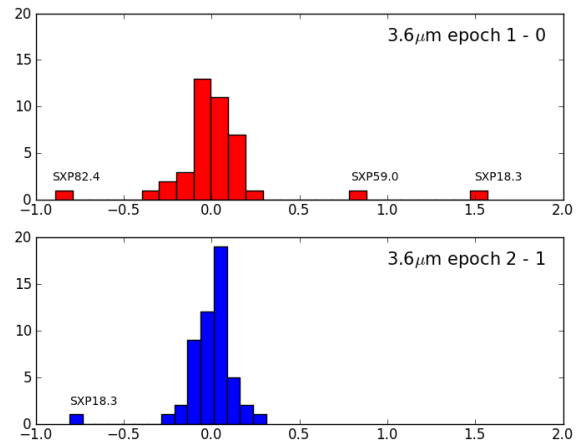


Figure 6. Magnitude difference between epochs showing the time variance in the brightness of SXP 18.3, SXP 82.4 and SXP 59.0 in the $3.6 \mu\text{m}$ band.

those from the SAGE-SMC catalogue (Gordon et al. 2011) and the OGLE I band magnitude was converted to flux. Flux values for simple blackbodies of different temperatures were then calculated and these values plotted on the same diagram. This diagram indicates the variation in the average temperature of the circumstellar disk component SXP 18.3 over the 3 epochs. This object was observed to be at its brightest during epoch 0 and its faintest during epoch 1. The blackbody curve, however, suggests that SXP 18.3 is at its coolest during epoch 0 and its hottest during epoch 1. Thus this plot

Epoch	3.6 μ m mag	Error	4.5 μ m mag	Error	5.8 μ m mag	Error	I-band mag	Error
Epoch 0 (?? May 2005)	14.35	0.02	14.24	0.02	14.22	0.07	14.968	0.002
Epoch 1 (15 Jun 2008)	15.92	0.09	15.94	0.10	null	null	15.925	0.005
Epoch 2 (19 Sep 2008)	15.11	0.06	14.95	0.06	null	null	15.435	0.004
SAGE-Var epoch 1 (17 Aug 2010)	15.27	0.13	15.04	0.14	null	null	null	null
SAGE-Var epoch 2 (12 Sep 2010)	15.47	0.11	15.37	0.11	null	null	null	null
SAGE-Var epoch 3 (24 Dec 2010)	16.12	0.18	15.99	0.13	null	null	null	null
SAGE-Var epoch 4 (16 Jun 2011)	16.04	0.13	16.35	0.20	null	null	null	null

Table 1. Spitzer/IRAC magnitudes of SXP 18.3, plus the nearest I-band measurement in time from OGLE.

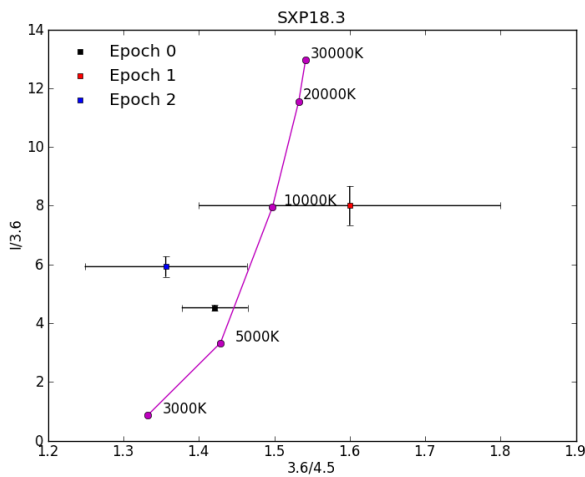


Figure 7. SXP 18.3 epoch flux ratio comparison with theoretical blackbody values. The vertical axis shows the ratio of the fluxes in the OGLE I-band ($0.8\mu\text{m}$) to the IRAC ($3.6\mu\text{m}$). The horizontal axis shows the flux ratio of the two IRAC bands ($3.6\mu\text{m}$ and $4.5\mu\text{m}$)

implies that the object cools as it gets brighter and the warms up again as the I-band declines. Since the far-IR emission is primarily from the circumstellar disk which is believed to be optically-thick, then the brighter state almost certainly indicates a larger disk size which is, on average, cooler than the smaller, though less-bright disk.

3.4 H α Equivalent Widths

H α is emitted from the circumstellar disk that surrounds the Be stars and is therefore another good probe of the disc. The equivalent width (EW) of the H α emission line was plotted against orbital period for each of the SXP systems with confirmed values - see Figure 8. The H α EW and the orbital period show a strong correlation with a Pearson Correlation coefficient of $R=0.644$ (corresponding to a probability of 9.4×10^{-5} that the correlation is random). This is a much stronger result than previously reported and agrees with that found by Reig, Fabregat & Coe (1997) for the separate population of Be/X-ray systems in the Milky Way. This correlation is thought to show evidence for truncated circumstellar discs (Dachs et al. 1986) arising from interaction with the orbiting neutron star. The positive correlation between H α and orbital period suggests that systems with larger orbital periods have larger H α values and therefore can sustain much larger discs. The linear best fit to all the data is shown in Figure 8 as a solid line and gives the relationship:

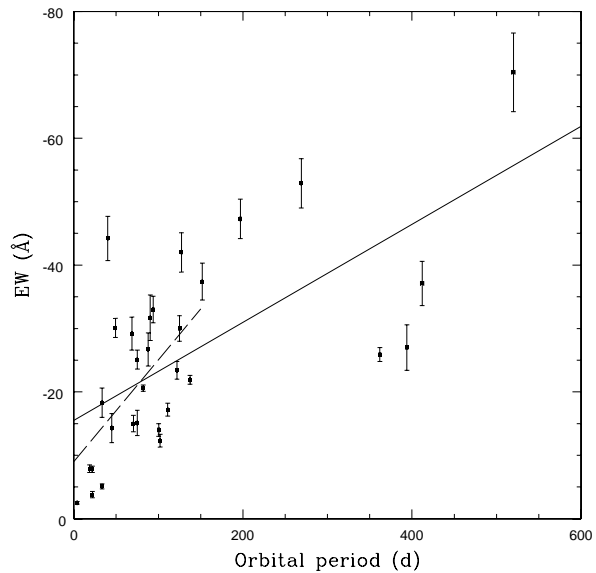


Figure 8. Orbital period plotted against H α Equivalent Width (EW) for SXP objects. The linear best fit line to all the data is shown (solid line), and the fit to just the data with $P_{orb} \leq 150d$ (dashed line). Errors bars are shown for both parameters, though fractionally very small for the orbital period.

$$H\alpha EW(\text{\AA}) = [-0.08 \times P_{orb}] - 15.5 \quad (1)$$

P_{orb} is the orbital period in units of days. There is a strong suggestion that this best fit line is over-estimating the H α EW at lower orbital periods, so a fit to only those points with a $P_{orb} \leq 150d$ is also shown as a dashed line. This gives a slightly lower correlation coefficient of $R=0.51$ for just those points and the relationship:

$$H\alpha EW(\text{\AA}) = [-0.16 \times P_{orb}] - 9.7 \quad (2)$$

Reig, Fabregat & Coe (1997) suggested this relationship arises from the disc of the Be star being truncated by the neutron star during its orbit. This implies that the size of the circumstellar disk in Be/X-ray systems should, on average, be smaller than those in isolated Be stars. To investigate this further the distribution of H α EW values for our SXP sources presented in Table 4 is shown in Figure 9. For comparison, the H α EW values from the catalogue of isolated Be stars in the SMC (Martayan et al. 2007) is also shown in this figure. The figure strongly suggests that, indeed, the EW values of the SXP population are, on average, lower than those of the

isolated Be star population. The mean value of the SXP sample is -27\AA and that of the isolated Be stars -40\AA . Furthermore, a Kolmogorov-Smirnov test of the two populations gives a probability of 0.9% that they are drawn from the same population.

A more direct test of this proposed physical link between the size of the neutron star orbit, a , and the size of the circumstellar disk, R_{cs} , would be to determine both of these parameters for each system and then see if a correlation exists. To determine the size of the circumstellar disk the $H\alpha$ EW values presented in Table 4 were used and inserted into the relationship from Hanuschik (1989):

$$\log\left(\sqrt{7}\frac{R_{OB}}{R_{cs}}\right) = [-0.32 \times \log(-EW)] - 0.2 \quad (3)$$

In this expression R_{OB} is the radius of the Be star determined from the individual spectral types given for each source in Table 4, and EW is the $H\alpha$ EW values in \AA .

The size of the semi-major axis, a , of the neutron star orbit may be determined from Kepler's Third Law:

$$a = \left[\frac{P_{orb}^2 G(M_{ns} + M_{OB})}{4\pi^2}\right]^{1/3} \quad (4)$$

where M_{OB} is the mass of the specific Be star determined from the given spectral type, M_{ns} is the mass of the neutron star (assumed here to be $1.4M_{\odot}$), and P_{orb} is the orbital period.

Using those two equations the sizes of the disk and the orbit were calculated for each source and the results are presented in Figure 10. It is clear that there is a strong correlation between these two basic physical parameters - the Pearson correlation coefficient, $R=0.74$. This corresponds to a probability of only 1×10^{-5} that there is no correlation; almost an order of magnitude stronger support for a relationship than is seen in the secondary characteristics plotted in Figure 8.

A simple best fit to the data is also shown in Figure 10. Both linear and quadratic functions were explored and the best fit was found to be the following expression to determine the size of the orbital semi-major axis in metres, a , as a function of the size of the circumstellar disk, R_{cs} , also in metres:

$$a = (7 \times 10^{-12})(R_{cs})^2 + 0.4524R_{cs} + (4.30 \times 10^{10}) \quad (5)$$

This equation implies that the size of the orbit is 1.5–2.0 times that of the circumstellar disk, consistent with the concept that the neutron star is normally orbiting outside the circumstellar disk.

We note in passing that discrepancies between stellar classification and observed luminosities, plus inferred masses & temperatures, have been reported for HMXB companions by Conti (1978) and Kaper (2001). However, changing the Be star mass by 2–3 M_{\odot} in Equation 4 has less than a 5% effect on the value for the semi-major axis and is, therefore, unimportant in this context.

It now seems beyond question that disk truncation is occurring in systems with neutron star companions.

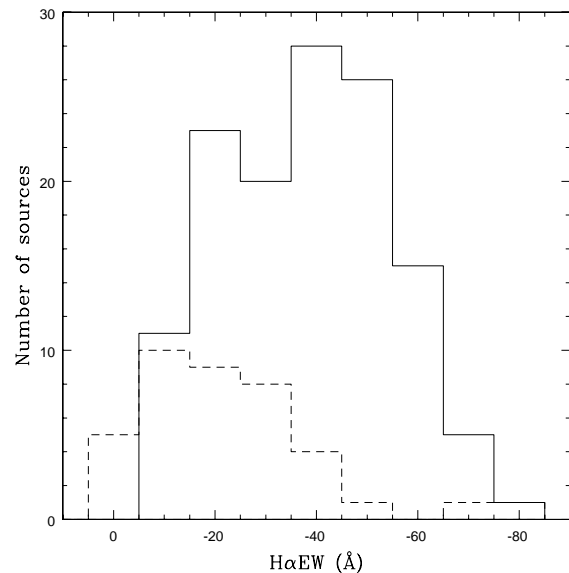


Figure 9. Distribution of $H\alpha$ EW values for a sample of single Be stars in the SMC (solid line) (Martayan et al. 2007), compared to the same parameter for the sample of SXP sources presented in this work (dashed line).

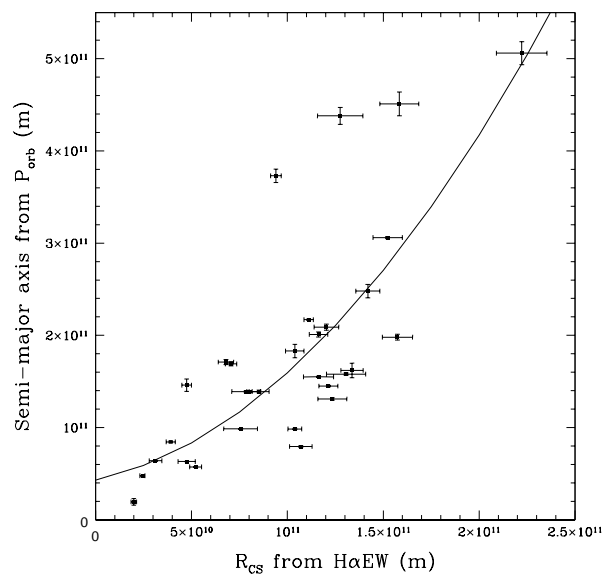


Figure 10. This figure shows the size determination in metres of the semi-major axis of the neutron star orbit (y-axis) and the size of the circumstellar disk (x-axis) for a sample of 31 SXP sources. The continuous line is a best fit quadratic function given in Equation 5.

4 CONCLUSIONS

This work presents the first large-scale, coherent sample of Be/X-ray sources in the Small Magellanic Cloud. Since this sample matches, or even exceeds in number the Milky Way sample, it provides an excellent astrophysical test bed for binary evolution and accretion processes. This is made even more effective because the coherent location of all these sources, with a well-defined distance and interstellar absorp-

tion, means that many of the issues arising from similar studies of Galactic objects are avoided. Therefore it is expected that this SMC population will provide an extremely useful astrophysical sample for testing future theoretical work.

5 ACKNOWLEDGEMENTS

We are grateful to Christian Knigge for re-running the KMM test on the revised SMC pulsar sample. We are also grateful to David Reibel for providing the results of the Spitzer SAGE-Var observations of SXP 18.3 before they became public.

REFERENCES

- Bartlett E. S., Clark J. S., Coe M. J., Garcia M. R., Uttley P., 2013, *MNRAS*, 429, 1213
- Bird A. J., Coe M. J., McBride V. A., Udalski A., 2012, *MNRAS*, 423, 3663
- Bolatto A. D. et al., 2007, *ApJ*, 655, 212
- Bonanos A. Z. et al., 2010, *AJ*, 140, 416
- Chaty S., Rahoui F., 2012, *ApJ*, 751, 150
- Cheng Z.-Q., Shao Y., Li X.-D., 2014, *ApJ*, 786, 128
- Coe M. J., Angus R., Orosz J. A., Udalski A., 2013, *MNRAS*, 433, 746
- Coe M. J., Bartlett E. S., Bird A. J., Haberl F., Kennea J. A., McBride V. A., Townsend L. J., Udalski A., 2015, *MNRAS*, 447, 2387
- Coe M. J., Edge W. R. T., Galache J. L., McBride V. A., 2005, *MNRAS*, 356, 502
- Conti P. S., 1978, *A&A*, 63, 225
- Dachs J., Hanuschik R., Kaiser D., Rohe D., 1986, *A&A*, 159, 276
- Evans C. J., Howarth I. D., Irwin M. J., Burnley A. W., Harries T. J., 2004, *MNRAS*, 353, 601
- Gordon K. D. et al., 2011, *AJ*, 142, 102
- Hanuschik R. W., 1989, *APSS*, 161, 61
- Heger A., Fryer C. L., Woosley S. E., Langer N., Hartmann D. H., 2003, *ApJ*, 591, 288
- Kaper L., 2001, in *Astrophysics and Space Science Library*, Vol. 264, *The Influence of Binaries on Stellar Population Studies*, Vanbeveren D., ed., p. 125
- Kato D. et al., 2007, *PASJ*, 59, 615
- Klus H., Ho W. C. G., Coe M. J., Corbet R. H. D., Townsend L. J., 2014, *MNRAS*, 437, 3863
- Knigge C., Coe M. J., Podsiadlowski P., 2011, *Nature*, 479, 372
- Liu Q. Z., van Paradijs J., van den Heuvel E. P. J., 2005, *A&A*, 442, 1135
- Martayan C., Floquet M., Hubert A. M., Gutiérrez-Soto J., Fabregat J., Neiner C., Mekkas M., 2007, *A&A*, 472, 577
- Negueruela I., Okazaki A. T., 2001, *A&A*, 369, 108
- Rajoelimanana A. F., Charles P. A., Udalski A., 2011, *MNRAS*, 413, 1600
- Reig P., 2011, *APSS*, 332, 1
- Reig P., Fabregat J., Coe M. J., 1997, *A&A*, 322, 193
- Riebel D. et al., 2015, *ArXiv e-prints*
- Schurch M. P. E. et al., 2009, *MNRAS*, 392, 361
- Stella L., White N., Rosner R., 1986, 308, 669
- Townsend L. J., Coe M. J., Corbet R. H. D., Hill A. B., 2011, *MNRAS*, 416, 1556
- Udalski A., 2008, *Acta. Astron.*, 58, 187
- Zaritsky D., Harris J., Thompson I. B., Grebel E. K., Massey P., 2002, *AJ*, 123, 855

Table 2. X-ray properties of the Small Magellanic Cloud sources - Part 1. See text for detailed explanation of the contents.

Short ID	RA(2000)			Dec(2000)		Alternative name(s)	Pulse (secs)	Orbital (days)	Other (days)	Eccen <i>e</i>
	h	m	s	d	m					
SXP 2.16	?			?			2.16			
SXP 2.37	0	54	36.2	-73	40	35.00	SMC X-2	2.37	9.30	0.07±0.02
SXP 2.76	0	59	12.80	-71	38	44.00	RX J0059.2-7138	2.76	81.81	
SXP 3.34	1	5	9.00	-72	11	46.9	AX J0105-722, RX J0105.1-7211	3.34	10.72	1.099
SXP 4.78	0	52	11.00	-72	20	18.00	XTE J0052-723, - sky location unclear	4.78		
SXP 5.05	0	57	2.30	-72	25	55.00	IGR J00569-7226	5.05	17.20	0.16±0.02
SXP 6.62	0	54	46.30	-72	25	23.00	CXOU J005446.2-722523	6.62		
SXP 6.85	1	2	53.30	-72	44	35.00	XTE J0103-728, [SHP2000] SMC 100	6.85	22.00	0.26±0.03
SXP 6.88	0	54	46.30	-72	25	22.80	[MA93] 798	6.88	2.71	
SXP 7.78	0	52	5.64	-72	26	04.0	SMC X-3	7.78	44.80	
SXP 7.92	0	57	58.00	-72	22	29.50	CXOU J005758.4-722229, [SHP2000] SMC 75	7.92	35.61	
SXP 8.80	0	51	53.20	-72	31	48.80	RX J0051.8-7231,AzV 102	8.90	33.40	0.41±0.04
SXP 9.13	0	49	13.60	-73	11	37.80	AX J0049-732	9.13	40.10	
SXP 9.60	?			?			RXTE source sky location unclear	9.60		
SXP 11.5	1	4	42.30	-72	54	3.70	IGR J01054-7253, [M2002] SMC 59977	11.48	36.30	0.28±0.03
SXP 11.6	1	57	16.15	-72	58	32.60	IGR J015712-7259	11.60	35.40	
SXP 11.9	0	48	13.47	-73	22	3.10	XMMU J004813.9-732202, M[2002] SMC 10287	11.89		
SXP 15.3	0	52	13.98	-73	19	18.80	RX J0052.1-7319,	15.30	74.3	
SXP 16.6	?			?			RXTE pulsar - sky location unclear	16.60	33.70	
SXP 18.3	0	49	11.47	-72	49	37.60	XTE J0055-727, XMMU J004911.4-724939	18.37	17.79	0.43±0.03
SXP 22.1	1	17	40.60	-73	30	50.60	RX J0117.6-7330	83.7		
SXP 25.5	0	48	14.10	-73	10	4.00	XMMU J004814.1-731003	25.55	22.50	
SXP 31.0	1	11	8.40	-73	16	46.00	XTE J0111.2-7317	31.00	90.40	
SXP 46.6	0	53	55.20	-72	26	44.80	1WGA 0053.8-7226,XTE J0053-724	46.60	137.40	
SXP 51.0	?			?			RXTE pulsar - sky location unclear(=SXP 25.5?)	51.00		
SXP 59.0	0	54	56.20	-72	26	47.90	RX J0054.9-7226,XTE J0055-724	58.95	122.00	
SXP 65.8	1	7	12.60	-72	35	33.80	CXOU J010712.6-723533	65.80	111.00	
SXP 74.7	0	49	5.90	-72	50	55.00	RX J0049.1-7250, AX J0049-729	74.80	33.30	2.4
SXP 82.4	0	52	9.00	-72	38	3.30	XTE J0052-725	82.40	362.00	1.33
SXP 89.0	?			?			RXTE pulsar - sky location unclear	89.00		
SXP 91.1	0	50	56.90	-72	13	34.40	AX J0051-722 ,RX J0051.3-7216	91.10	88.00	
SXP 95.2	?			?			RXTE pulsar - sky location unclear	95.20		
SXP 101	0	57	27.0	-73	25	19.60	AX J0057.4-7325, RX J0057.3-7325	101.40	21.90	
SXP 138	0	53	23.80	-72	27	15.00	CXOU J005323.8-722715	138.00	125.00	

Table 3. X-ray properties of the Small Magellanic Cloud sources - Part 2. See text for detailed explanation of the contents. The last object in this table is technically in the Magellanic Bridge and therefore does not have an SXP nomenclature. No sources in this table have measured eccentricities, so that column is not included here.

Short ID	RA(2000)			Dec(2000)			Alternative name(s)	Pulse (secs)	Orbital (days)	Other (days)
	h	m	s	d	m	s				
SXP 140	0	56	5.80	-72	21	59.00	XMMU J005605.2-722200,2E0054.4-7237	140.10	197.00	
SXP 144	?			?			RXTE pulsar - sky location unclear	144.10	59.40	
SXP 152	0	57	50.30	-72	7	56.00	CXOU J005750.3-720756, [MA93]1038	152.10		
SXP 153	1	7	43.20	-71	59	53.90	XMMU J010743.1-715953	153.00	100.30	
SXP 169	0	52	55.30	-71	58	6.00	XTE J0054-720, AX J0052.9-7158	169.30	68.60	0.755
SXP 172	0	51	52.00	-73	10	34.00	AX J0051.6-7311, RX J0051.9-7311	172.40	68.8	
SXP 175	1	1	52.50	-72	23	34.00	RX J0101.8-7223 [MA93]1288	175.40	87.22	
SXP 202A	0	59	21.03	-72	23	17.30	1XMMU J005920.8-722316	202.00		
SXP 202B	0	59	28.68	-72	37	4.20	XMMU J005929.0-723703	202.00	224.6	
SXP 214	0	50	11.26	-73	0	26.10	XMMU J005011.2-730026	214.00		
SXP 264	0	47	23.30	-73	12	27.50	XMMUJ004723.7-731226, RXJ0047.3-7312,[MA]172	263.60	49.20	
SXP 265	1	32	51.50	-74	25	45.30	XMMSL1 J013250.6-742544	264.50	146.00	0.867
SXP 280	0	57	49.60	-72	2	36.20	AX J0058-72.0	280.40	127.30	
SXP 292	0	50	47.90	-73	18	17.0	CXOU J005047.9-731817	292.00		
SXP 293	0	58	12.57	-72	30	48.80	RX J0058.2-7231, XTE J0051-727	293.00	59.70	
SXP 304	1	1	2.90	-72	6	59.00	CXOU J010102.7-720658, [MA93]1240,RXJ0101.0-7206	304.50	520.00	0.26
SXP 323	0	50	44.70	-73	16	5.00	AX J0051-73.3,RXJ0050.7-7316	323.20		0.71
SXP 327	0	52	52.20	-72	17	15.10	[SHP 2000] SMC_45, XMMU J005252.1-721715	327.00	45.99	
SXP 342	0	54	3.90	-72	26	32.90	XMMU J005403.8-722632	342.00		
SXP 348	1	3	13.97	-72	9	14.80	SAX J0103.2-7209, RX J0103-722	349.90	93.90	
SXP 455	1	1	20.60	-72	11	19.20	RX J0101.3-7211, [MA 93] 1257	452.00	75.00	
SXP 504	0	54	55.90	-72	45	10.90	CXOU J005455.6-724510,RXJ0054.9-7245,AXJ0054.8-7244	503.00	269.00	5.3
SXP 523	1	2	47.00	-72	4	51.00	XMMU J010247.5-720450	522.00		
SXP 565	0	57	36.00	-72	19	34.00	CXOU J005736.2-721934, [MA93]1020	564.80	152.4	
SXP 645	0	55	35.20	-72	29	6.00	XMMU J005535.2-722906	645.00		
SXP 701	0	55	17.90	-72	38	53.00	XMMU 005517.9-723853	702.00	412.00	0.285
SXP 723	?		?				RXTE pulsar - sky location unclear	720.00		
SXP 726	1	5	55.20	-72	3	51.00	RX J0105.9-7203	726.00		
SXP 756	0	49	42.00	-73	23	14.70	AX J0049.4-7323, RX J0049.7-7323(?)	755.50	394.00	
SXP 893	0	49	29.85	-73	10	58.30	CXO J004929.7-731058	892.80		
SXP 967	1	2	6.70	-71	41	16.20	CXOU J010206.6-714115	967.00	101.4	
SXP 1062	1	27	45.95	-73	32	56.30	2dFS 3831	1063.00	656?	
SXP 1323	1	3	37.40	-72	1	34.10	RX J0103.6-7201, [MA93] 1393, [M2002] SMC 56901	1323.00		26.2,0.88, 0.41
SXP 4693	0	54	46.30	-72	25	22.80	CXOU J005446.3-722523	4693.00		
0157-7259	1	57	16.15	-72	58	32.6	IGR J015712-7259 Bridge object	11.60	35.1?	

Table 4. Small Magellanic Cloud Be/X-ray systems: optical/IR properties. The JHK values come from the IRSF catalogue of Kato et al. (2007) and the longer IR wavelength data from Spitzer (Gordon et al. 2011). The $H\alpha$ Equivalent Width (EW) values come from Klus et al. (2014). X-ray sources with no identified optical counterparts are not included in this table.

ID	Spect Class	V mag	Opt col B-V	J mag	J err	H mag	H err	K mag	K err	3.6 μ m mag	3.6 μ m err	4.5 μ m mag	4.5 μ m err	5.8 μ m mag	5.8 μ m err	8.0 μ m mag	8.0 μ m err	IR col J-K	$H\alpha$ EW(\AA)	$H\alpha$ error
SXP 0.72	B0 I	13.15	-0.14	13.62	0.02	13.65	0.01	13.66	0.02	13.38	0.07	13.23	0.04	13.21	0.08	13.01	0.09	-0.04	-2.5	0.2
SXP 2.37	O9.5III-V	16.64	0.06	15.1	0.02	15.01	0.02	14.85	0.03	14.29	0.06	14.19	0.05	13.94	0.13	-	-	0.25	-7.9	0.6
SXP 2.76	B1IIIe	14.01	0.06	13.96	0.02	13.84	0.02	13.63	0.02	13.37	0.06	13.14	0.04	12.87	0.08	12.71	0.09	0.33	-20.6	0.5
SXP 3.34	B1-B2 III-V	15.63	-0.01	15.66	0.01	15.56	0.02	15.45	0.04	14.99	0.07	14.7	0.05	14.29	0.17	-	-	0.21	-85.2	8.9
SXP 4.78				14.54	0.01	14.58	0.01	14.65	0.02	14.52	0.1	14.71	0.06	14.43	0.16	-	-	-0.11	?-43.7	1.1
SXP 6.62				15.32	0.01	15.17	0.02	14.92	0.02	14.46	0.06	-	-	13.85	0.12	-	-	0.40		
SXP 6.85	O9.5-B0 IV-V	14.60		14.82	0.02	14.74	0.02	14.57	0.02	14.16	0.05	14.1	0.07	14.16	0.16	-	-	0.25	-3.8	
SXP 7.78	B1-B1.5 IV-V	14.90	0.00	14.8	0.01	14.7	0.01	14.5	0.01	14.09	0.05	13.93	0.06	13.79	0.11	-	-	0.30	-14.3	2.3
SXP 8.80	O9.5-B0 IV-V	14.87	-0.27	14.7	0.01	14.64	0.02	14.56	0.02	14.17	0.05	14.07	0.09	13.98	0.12	-	-	0.14	-5.1	0.4
SXP 9.13	B1-B3 IV-V	16.50	0.10	16.23	0.02	16.02	0.03	15.8	0.04	15.37	0.04	15.08	0.06	-	-	-	-	0.43	-44.2	3.5
SXP 11.5	O9.5-B0 IV - V	14.80	0.00	14.21	0.08	13.75	0.06	13.74	0.04	-	-	13.3	0.04	13.26	0.09	13.17	0.1	0.47		
SXP 11.9				14.67	0.01	14.62	0.01	14.53	0.02	14.42	0.07	14.28	0.07	14.06	0.15	-	-	0.14		
SXP 15.3	O9.5-B0 III-V	14.70	-0.01	14.4	0.02	14.3	0.01	14.12	0.01	13.6	0.05	13.45	0.05	13.24	0.09	13.12	0.1	0.28	-25.1	1.5
SXP 18.3				16.00		16.05	0.02	16.03	0.03	16.13	0.05	15.92	0.09	15.94	0.1	-	-	-0.08		
SXP 22.1	O9.5-B0 III-V	14.20	-0.04	14.18	0.01	14.11	0.02	13.87	0.03	13.35	0.04	13.23	0.04	13.05	0.08	12.74	0.07	0.31	-25.1	2.5
SXP 25.5	B1.5e	15.70	0.01	15.68	0.02	15.68	0.02	15.64	0.04	15.33	0.05	15.17	0.12	-	-	-	-	0.04		
SXP 31.0	B0.5-B1 V	15.50	-0.10	15.4	0.02	15.3	0.02	15.14	0.03	14.41	0.05	14.14	0.05	-	-	-	-	0.26	-31.7	3.6
SXP 46.6	O9.5-B1 IV-V	14.70	-0.07	14.72	0.01	14.6	0.02	14.45	0.02	13.62	0.12	13.62	0.1	13.37	0.12	-	-	0.27	-21.9	0.7
SXP 59.0	O9V	15.30	-0.04	15.52	0.01	15.47	0.02	15.39	0.04	15.32	0.06	15.02	0.08	-	-	-	-	0.13	-23.4	1.4
SXP 65.8	B1-B1.5III-III	15.00		15.64	0.01	15.49	0.02	15.37	0.04	15.03	0.07	-	-	-	-	-	-	0.27	-17.2	
SXP 74.7	B3V	16.90	0.09	16.72	0.03	16.54	0.04	16.32	0.06	15.78	0.11	15.57	0.14	-	-	-	-	0.40	-18.3	2.3
SXP 82.4	B1-B3III-V	15.00	0.14	15.59	0.01	15.52	0.02	15.47	0.05	14.37	0.06	14.19	0.08	13.8	0.13	-	-	0.12	-25.9	1.1
SXP 91.1	B0.5III-V	15.10	-0.08	14.73	0.02	14.63	0.01	14.37	0.02	13.84	0.05	13.67	0.06	13.47	0.09	13.1	0.08	0.36	-26.7	2.6
SXP 101	B3-B5 Ib-II			15.64	0.01	15.57	0.02	15.38	0.03	15.15	0.06	15	0.08	-	-	-	-	0.26	-7.8	
SXP 138	B1-B2 IV-V	16.20	-0.09	16.1	0.02	15.98	0.03	15.89	0.06	15.43	0.07	15.18	0.08	-	-	-	-	0.21	-30.0	2.0
SXP 140	B1V	15.90	-0.04	15.34	0.01	15.26	0.02	15.09	0.03	14.95	0.06	14.64	0.07	-	-	-	-	0.25	-47.3	3.1
SXP 152	B1-B2.5 III-V	15.70	-0.03	15.36	0.01	15.19	0.02	14.98	0.02	14.51	0.06	14.31	0.06	14.24	0.13	-	-	0.38	-17.3	1.7
SXP 153	B2IV-Ve.			16.4	0.02	16.21	0.02	16	0.06	15.13	0.06	14.87	0.09	-	-	-	-	0.40	-14.0	1.0
SXP 169	B0-B1 III-V	15.50	0.02	15.29	0.01	15.17	0.01	14.93	0.02	14.58	0.06	14.45	0.06	14.07	0.13	-	-	0.36	-29.2	2.6
SXP 172	O9.5-B0 V	14.50	-0.07	14.61	0.01	14.53	0.01	14.44	0.02	13.93	0.04	13.72	0.06	13.61	0.08	13.3	0.07	0.17	-15.0	1.3
SXP 175		14.60	-0.04	14.82	0.01	14.73	0.02	14.53	0.02	14.04	0.04	13.71	0.06	13.5	0.07	13.32	0.09	0.29		
SXP 202A	B0-B1 V	15.10	-0.24	14.72	0.01	14.65	0.01	14.5	0.02	14.01	0.03	13.74	0.04	13.56	0.07	13.32	0.07	0.22	-18.1	
SXP 202B				15.26	0.01	15.05	0.01	14.82	0.02	14.38	0.07	14.13	0.07	14.04	0.15	-	-	0.44		
SXP 214	B2-B3 III			15.32	0.02	15.38	0.02	15.37	0.02	15.26	0.05	15.35	0.08	-	-	-	-	-0.05		
SXP 264	B1-B1.5 V	15.85	0.00	15.92	0.02	15.75	0.02	15.54	0.03	14.92	0.06	14.85	0.08	-	-	-	-	0.38	-30.1	1.7
SXP 265	B1-2 II-IVe	15.00		15.92	0.07	16.12	0.08	16.7	0.11									-0.78		
SXP 280	B0-B2 III-V	15.70	-0.12	15.26	0.01	15.05	0.01	14.76	0.02	14.46	0.06	14.2	0.05	14.47	0.16	-	-	0.50	-42.0	3.1
SXP 292	O9-B2 III-V	15.1		15.09	0.01	14.99	0.02	14.85	0.02	14.358	0.05	14.292	0.076	13.863	0.106	-	-	-31.0		
SXP 293	B0IIIe	14.90		14.53	0.01	14.35	0.01	14.14	0.02	13.7	0.04	13.46	0.04	13.23	0.08	13.12	0.1	0.39		
SXP 304	B0-B2 III-V	15.70	-0.04	15.56	0.02	15.4	0.02	15.13	0.03	14.69	0.05	14.37	0.07	14.47	0.14	-	-	0.43	-70.4	6.2
SXP 323	B0-B0.5 V	15.40	-0.04	15.2	0.02	15.1	0.02	14.9	0.02	14.35	0.05	14.16	0.04	13.87	0.13	13.63	0.11	0.30	-30.9	1.1
SXP 327	B2??			16.55	0.02	16.27	0.02	16.14	0.04	15.66	0.08	15.65	0.1	-	-	-	-	0.41		
SXP 342				15.21	0.02	15.17	0.02	15.03	0.03	-	-	14.95	0.08	-	-	-	-	0.18		
SXP 455	B0.5-B2 III-V	15.50	-0.07	16.03	0.02	15.99	0.02	15.89	0.05	15.55	0.07	15.54	0.07	-	-	-	-	0.14	-15.1	2.0
SXP 504	B1 III-V	14.99	-0.02	14.77	0.01	14.63	0.01	14.4	0.01	13.89	0.04	-	-	13.43	0.08	13.07	0.09	0.37	-52.9	3.9
SXP 523		16.00	-0.25	16.58		16.52		16.61										-0.03		
SXP 565	B0-B2 IV-V	15.97	-0.02	15.77	0.01	15.6	0.01	15.35	0.03	14.72	0.07	14.48	0.05	14.28	0.14	-	-	0.42	-37.4	2.9
SXP 645				15.11	0.01	15.09	0.01	15.06	0.03	14.1	0.06	13.79	0.05	13.69	0.09	13.29	0.11	0.05		
SXP 701	O9.5 V	16.00	0.03	15.6	0.02	15.41	0.02	15.21	0.02	14.45	0.07	14.12	0.07	14.03	0.15	-	-	0.39	-37.1	3.5
SXP 726		15.60	-0.02	15.47	0.01	15.37	0.02	15.04	0.03	14.56	0.05	14.38	0.05	14.33	0.15	-	-	0.43		
SXP 756	O9.5-B0.5 III-V	14.98	0.05	14.57	0.01	14.4	0.01	14.16	0.02	13.53	0.04	13.3	0.04	13.03	0.07	12.95	0.07	0.41	-27.0	3.6
SXP 893	B1e			15.75	0.02	15.46	0.02	15.22	0.02	14.66	0.05	14.44	0.07	14.15	0.1	-	-	0.53		
SXP 967	B0-B0.5 III-V	14.60		14.46	0.02	14.39	0.01	14.24	0.02	13.63	0.05	13.41	0.04	13.25	0.08	12.98	0.09	0.22	-12.3	
SXP 1062	B0-0.5III			14.17	0.01	14.07	0.01	13.88	0.02	13.41	0.05	13.2	0.05	12.89	0.08	12.65	0.06	0.29		
SXP 1323	B0 III-V	14.60		14.6	0.02	14.51	0.02	14.34	0.02	14.07	0.05	13.88	0.04	13.71	0.07	-	-	0.26	-17.1	1.5
SXP 4693		15.40	0.14	15.32	0.01	15.17	0.02	14.92	0.02	14.46	0.06	-	-	13.85	0.12	-	-	0.40		